RESEARCH

Blind reconfigurable intelligent surface-aided fixed non-orthogonal multiple access for intelligent vehicular networks

Vinoth Babu Kumaravelu[1], Poongundran Selvaprabhu[1], Dong Seog Han[2*], Md. Abdul Latif Sarker[3], Velmurugan Periyakarupan Gurusamy Sivabalan[4], Thiruvengadam Sundarrajan Jayaraman[4], Arthi Murugadass[5] and C. Suganthi Evangeline[6]

*Correspondence:
dshan@knu.ac.kr

[1] Department of Communication Engineering, School of Electronics Engineering, Vellore Institute of Technology, Vellore, Tamil Nadu, India
[2] School of Electronic and Electrical Engineering, Kyungpook National University, Daegu 41566, Republic of Korea
[3] Centre for ICT & Automotive Convergence, Kyungpook National University, Daegu 41566, Republic of Korea
[4] Department of Electronics and Communication Engineering, Thiagarajar College of Engineering, Madurai, Tamil Nadu, India
[5] Department of Computer Science and Engineering (AI&ML), Sreenivasa Institute of Technology and Management Studies, Chittoor, Andhra Pradesh, India
[6] Department of Electronics and Communication Engineering, Sri Eshwar College of Engineering, Coimbatore, Tamil Nadu, India

Abstract

In intelligent vehicular networks, vehicles should be able to communicate with their surroundings while traveling. This results in more efficient, safer, and comfortable driving experiences, as well as new commercial prospects in a variety of industries. Connected vehicles and autonomous vehicles expect 100% reliable connectivity without any compromise in quality. However, due to challenges such as difficult channel terrains in urban scenarios and dead zones, the reliability of current vehicle-to-infrastructure (V2I) and vehicle-to-vehicle communication systems cannot be guaranteed. The performance of vehicular networks can be considerably enhanced with reconfigurable intelligent surfaces (RIS). Non-orthogonal multiple access (NOMA) allows for massive connectivity with the surroundings. In vehicular networks, the RIS-assisted NOMA can ensure regulated channel gains, better coverage, throughput, and energy efficiency. In this work, a blind RIS-assisted fixed NOMA (FNOMA) system is proposed for a downlink V2I scenario. The closed-form analytical outage probability and throughput expressions are derived by considering RIS as an intelligent reflector and as a roadside unit. It is observed that the analytical and Monte Carlo simulation results are closely related. In simulations, it has been discovered that RIS-assisted FNOMA outperforms the traditional NOMA variants in terms of outage and throughput. Even without precise channel knowledge, blind RIS transmission outperforms traditional NOMA variants due to huge array gain. The increase in the number of reflective elements also results in a significant improvement in signal-to-noise ratio gains.

Keywords: Fixed non-orthogonal multiple access (FNOMA), Next-generation networks, Outage probability, Reconfigurable intelligent surfaces (RIS), Throughput, Vehicle-to-infrastructure (V2I)

1 Introduction

In spite of a worldwide pandemic in 2020, 38,680 persons died in vehicular crashes [1]. By 2030, the World Health Organization hopes to have cut down on vehicular-related injuries and fatalities by 50% [2]. Vehicular ad hoc network (VANET) has received considerable interest from academic, government, and automotive industries as a critical

component of intelligent transportation system (ITS) to improve efficiency and safety of road. To enable safety applications such as lane change warnings, collision avoidance, and harsh braking warnings, data such as the vehicle's position and speed must be broadcasted to nearby vehicles on frequent intervals [3]. Low latency and high reliability are required for safety applications. Non-safety applications such as internet access, online games, online payments, and infotainment are also expected to be supported by VANET [4]. Users of infotainment services expect to have a more efficient and enjoyable driving experience. The timely and dependable distribution of this data is critical for a variety of safety applications. In order to get services related to road safety, traffic management, infotainment, and environmental monitoring for autonomous driving, vehicles must maintain a seamless connection with infrastructure units known as roadside units (RSU). Even though VANET is capable of providing all services to its users, ensuring connectivity and signal propagation remains a challenge. The unstable network topologies prevent reliable vehicle-to-everything (V2X) communication, which has become a challenging investigation direction.

For connected autonomous vehicle applications, V2X communications must be supported. Because these communications rely on the wireless channel's signal-to-noise ratio (SNR) and fading characteristics, higher frequency bands must be explored to compensate for the spectrum demand in the sub-6 GHz band. The millimeter wave (mmWave) is utilized in the new radio (NR) concept, which is supported in third-generation partnership project (3GPP) Release-15 is used for cellular-V2X communication (C-V2X). When there is high path loss and low SNR values, it also imposes some limits on reliability issues. Theoretically, the options proposed by the scientific community to address these challenges are to enhance transmit power and minimize the distance between transmitter and receiver. However, this is not feasible in practice. As a result, software-controlled reconfigurable intelligent surfaces (RIS) are offered as a way to increase V2X communication reliability, and they will be widely adopted in sixth-generation (6G) networks [5]. Future self-driving vehicles will require reliable and better quality connectivity between vehicles and between vehicles and infrastructure. The performance of VANET can be considerably enhanced with the RIS [6, 7].

Without the use of a dedicated energy source, a large number of tiny, low-cost passive elements make up RIS, which reflect the incoming signal with a suitable phase shift [8, 9]. RIS functions like mirrors that beamform the incoming signals to the intended users. It has been demonstrated that RIS can improve data rate performance as well as mitigate the Doppler effect of high-mobility users [10]. With the help of RIS, the propagation environment can be controlled [11, 12]. The placement of RIS is energy efficient and environmentally friendly. RIS has the compatibility to work with full-duplex relays, non-orthogonal multiple access (NOMA), index modulation (IM), simultaneous wireless information and power transfer (SWIPT), VANET, etc. Due to the above benefits, RIS has become one of the promising technologies of 6G networks [13].

Beamforming, range extension, positioning, and remote sensing are all potential use cases for RIS in VANET communication [14]. Some of the VANET safety applications that leverage the beamforming concept are incident detection, hazardous warning, cooperative collision avoidance, and trajectory alignment. Range extension, support for information interchange in autonomous driving, accurate data, and platooning are

all incorporated features. It also covers non-safety applications including video sharing, traffic information sharing, customized information, location-aware information, and environmental factor detection, in addition to the RIS's potential use cases stated above.

To improve the spectral efficiency and massive connectivity of RIS, power-domain NOMA can be integrated with RIS. In NOMA, the signals corresponding to different users are superimposed in power domain so that the spectrum is exploited more efficiently [15–17]. The users are explored opportunistically based on the channel conditions [18]. In a VANET, an RSU should be able to accommodate a larger number of vehicles at the same time while meeting their quality of service (QoS) demands. As a result, NOMA's integration with RIS is important.

A sample scenario for downlink RIS-assisted V2I is shown in Fig. 1. Because of the blockage, the RSU may deliver very poor services to the vehicles. However, the RIS on the building creates a virtual line of sight (LoS) between the RSU and the vehicles. The array gain and diversity gain benefits are improved by the reflective elements, resulting in improved received signal quality. Figure 2 depicts an example of RIS-assisted vehicle-to-vehicle (V2V). A source vehicle wants to exchange information with a destination vehicle. However, the vehicle in between may be a blockage or eavesdropper. The RIS in the propagation environment functions as an intelligent reflector (IR), allowing for high-quality, seamless communication between source and destination vehicles.
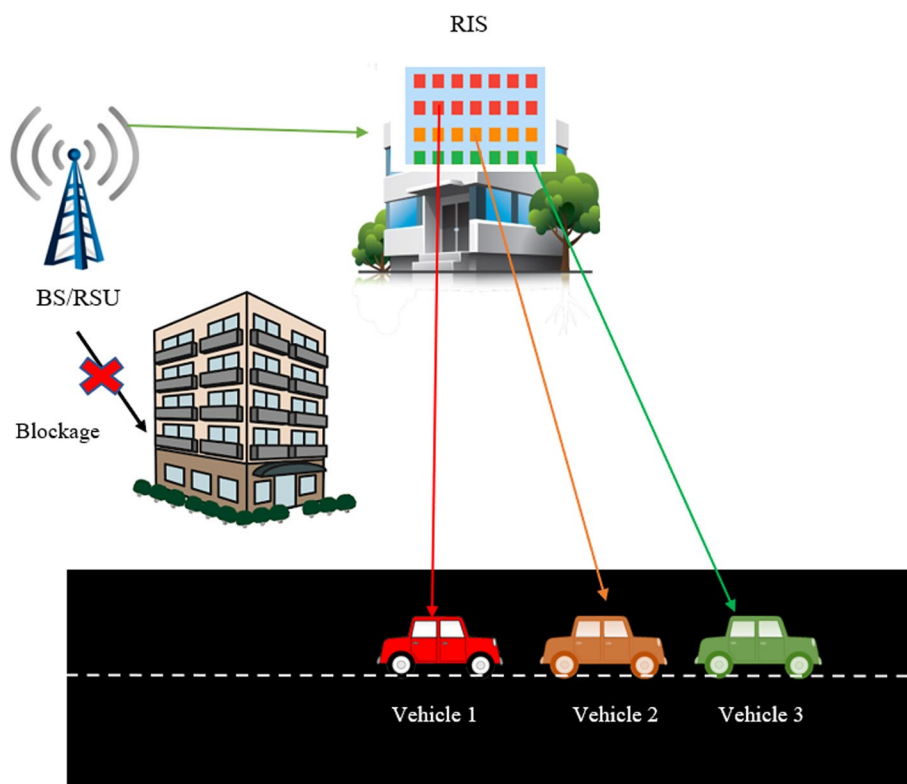

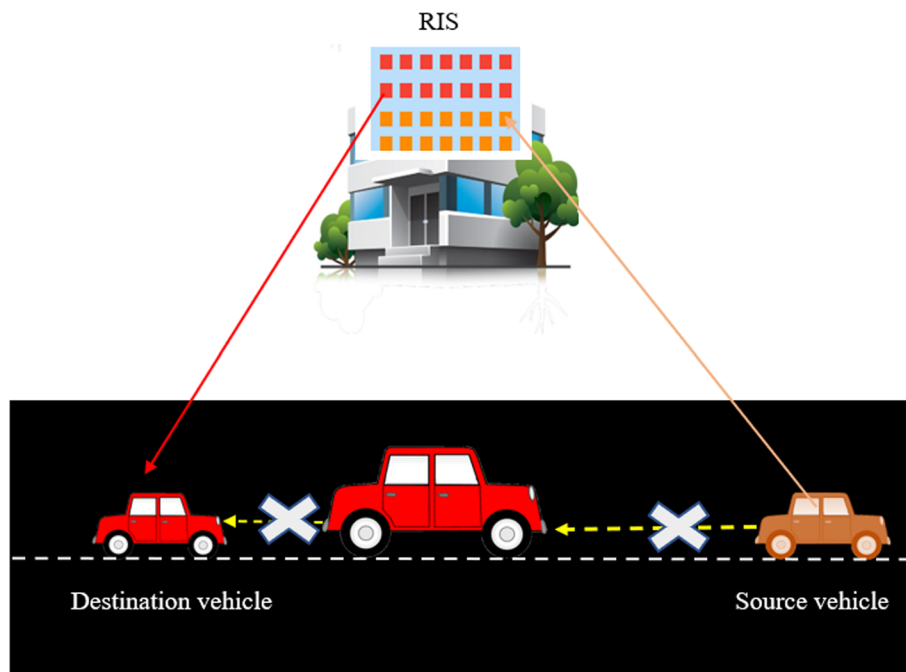**Fig. 1** A sample scenario for downlink RIS-assisted V2I

Fig. 2 A sample scenario for RIS-assisted V2V

1.1 Related work

RISs have been studied extensively for use in wireless communication, including RIS-assisted unmanned aerial vehicle (UAV) systems, RIS-assisted multicast communication, and RIS-assisted MIMO [19]. However, there have been very few studies on RIS-assisted vehicular communication. The use of RIS for secure vehicle communications was examined in [20]. The secrecy outage probability of two vehicular scenarios, V2V and V2I, was derived. In V2V, RIS served as a relay node, while in V2I, it served as a receiver. In [7], the expressions for secrecy outage probability was derived by utilizing series expansion and central limit theorem (CLT). The numerical results suggested that RIS could significantly reduce the outage probability for the vehicles in its vicinity. The secrecy outage probability was the function of the number of reflective elements. The performance could be enhanced by increasing the number of RIS elements.

In [21], the authors suggested a QoS-driven spectrum sharing scheme for RIS-assisted vehicular networks in order to maximize the sum capacity of V2I links utilized for high-rate content delivery, while also ensuring the reliability of V2V links utilized for the transmission of safety data. The authors of [22] modeled inter-vehicle links with Fox's H-function and studied outage probability and effective rate expressions using a passive RIS-equipped beacon vehicle. The authors of [23] modeled vehicular networks using RIS as an access point (AP). The instantaneous data rate was calculated as a function of the beam width, vehicle speed, and distance.

In [24], the weighted sum capacity of all the users was maximized by jointly designing the beamforming at base station (BS) and phase shift angles at RIS. Through the joint optimization of beamforming at the BS and phase shifts at the RIS, the blockage in the links from the BS/satellite to multiple users was addressed in a hybrid satellite-terrestrial relay network [25]. The total transmit power of the BS and satellite was minimized,

Kumaravelu *et al. J Wireless Com Network*   (2023) 2023:83

Page 5 of 25

while users' QoS requirements were met. In [26], a physical layer security (PLS) method for cognitive satellite-terrestrial integrated network (STIN) was developed to combat multiple eavesdropper threats. Active RIS was used in this work to alter the amplitude and phase of the signal being received. The proposed method strived to maximize the secrecy rate while meeting the transmit power constraint and the interference threshold. When compared to passive RIS and no RIS systems, active RIS eliminated the impact of double fading and improved security performance. The effectiveness of RIS-assisted communication systems in improving the security and spectrum efficiency of multiple users was examined in [27].

Because V2X communication involves the exchange of a large volume of data, it causes increased latency and unequal connectivity. When compared to orthogonal multiple access (OMA) approaches, NOMA techniques exhibit better spectrum efficiency and lower latency [28]. Massive connectivity with the same resources is possible with NOMA. In exchange for additional receiver complexity, it also incorporates controllable interference to superpose different vehicle signals. In [18], the closed-form outage probability expressions for ordered NOMA (ONOMA) uplink and downlink communication systems were derived using generalized fading channels. The authors studied both statistical and instantaneous channel state information (CSI)-based ordering schemes. The performance of cell-edge users could be improved in cooperative NOMA (CNOMA) [29] and SWIPT-CNOMA [30] by compromising the performance of nearby users. In [31], NOMA-assisted cooperative relaying was presented for reliable communication. In this scenario, the source and relay transmit a superimposed signal at the first- and second-time slots of the cooperative communication. The exact analytical closed-form outage probability expressions were derived considering Rayleigh fading channel and imperfect successive cancellation decoding. The outage probability of the presented scheme was compared with the conventional cooperative relaying-assisted NOMA.

In [32], a joint optimization design for NOMA-assisted STIN was developed. To maximize the sum rate of STIN, while satisfying the power constraints of each antenna and the QoS needs of satellite and cellular users, a constrained optimization problem was defined. To accommodate more than two users, a unique user clustering was also presented. NOMA and cognitive radio are two potential technologies that can effectively use satellite resources. The effectiveness of NOMA-aided STIN, when numerous primary users share the spectrum, was examined in [33]. The outage probability and sum capacity expressions were developed considering the interference limits enforced by multiple primary users. The NOMA-aided cognitive satellite-UAV terrestrial network was presented in [34] to improve spectrum efficiency and facilitate exponential user growth. Even with imperfect channel knowledge, the joint power allocation and sub-channel assignment algorithm improved the transmission performance of the recommended system. In [35], the authors proposed a novel index-coded NOMA to increase VANET spectral efficiency. The authors of [36] employed the NOMA technique for decentralized V2V communication, with a focus on channel modeling.

The outage behavior of a STAR-RIS-enabled cognitive non-terrestrial UAV with NOMA was studied in [37] under Rician fading and perfect/imperfect successive interference cancellation (SIC) situations. The outage probability expressions for secondary vehicular users were derived by considering primary vehicular users'

as interference. The proposed scheme outperformed both the STAR-RIS-OMA and non-STAR-RIS schemes. The majority of the existing literature assumed RIS-IR configuration, in which the channels between the BS-RIS and the RIS-vehicle (user) were known in advance in order to compensate for channel distortions. It is difficult to have ideal channel knowledge of every vehicle in V2X applications. Many of the works assumed RIS between the BS and vehicles. Because it is passive, RIS can only reflect the signal that has been received in the desired direction. As a result, the received signal power at the RIS is very poor, and the benefits that have been conversed about for RIS are not practical. RIS was rarely considered near/at the BS or vehicles in the works.

The blind RIS-aided FNOMA framework was proposed in [38] with IR and AP configurations for uplink transmission. In [39], the blind RIS-assisted framework was investigated for ONOMA, where channel gains ascertain the vehicle decoding order. In both [38, 39], an optimization problem for power allocations was formulated to maximize the sum capacity of near and far users. Monte Carlo simulations were employed to validate the theoretical outage expressions. These systems outperformed conventional NOMA by $\approx$ 30% for 20 dB SNR and 32 reflective elements.

1.2 Contributions
Motivated by the benefits of RIS-assisted NOMA system for vehicular communication, the performance of blind RIS-assisted FNOMA for a downlink V2I is considered in the proposed work. The key contributions of this work are emphasized here.

- To address the aforementioned issues, blind RIS as an IR (RIS-IR)-assisted FNOMA and RIS as an RSU (RIS-RSU)-assisted FNOMA methods are proposed in this work.
- The closed-form analytical outage and throughput expressions for RIS-IR-FNOMA and RIS-RSU-FNOMA are derived.
- The derived analytical outage probability and throughput expressions are validated through extensive Monte Carlo simulations. There is a tight bound between the analytical and simulation results. This validates the accuracy of derived analytical expressions.
- The proposed RIS-assisted FNOMA and conventional NOMA variants are compared in terms of outage probability and throughput. The blind RIS-RSU-FNOMA is shown to perform comparably to the blind RIS-IR-FNOMA in terms of throughput and outage.

1.3 Organization
The rest of the manuscript is presented in the following order: The analytical closed-form outage probability and throughput expressions for the proposed blind RIS-IR-FNOMA and RIS-RSU-FNOMA methods are derived in Sect. 2. Extensive Monte Carlo simulations are used in Sect. 3 to validate the derived analytical expressions. Conclusions summarize the findings and suggest future research.

2 Methods

In this section, two different blind RIS-assisted FNOMA methods are proposed to reduce outage and increase throughput of both near and far vehicles. The blind configuration of RIS is practical since it does not require prior channel knowledge. In the first proposed method namely blind RIS-IR-FNOMA, FNOMA is combined with a blind RIS-IR configuration and the RIS is deployed far from the transmitter and receiver in the IR configuration. In the second proposed method, namely blind RIS-RSU-FNOMA, FNOMA is combined with a blind RIS-RSU configuration. RIS is positioned very close to the RSU. In both methods, passive RIS is used. Passive RIS can only reflect the received signal in the desired direction. Closed-form analytical expressions are derived for outage and throughput for both proposed methods.

2.1 Blind RIS-IR-FNOMA

The conceptual diagram of blind RIS-IR-FNOMA for a downlink V2I scenario [20] is shown in Fig. 3. RIS with N reflecting elements is mounted on the wall of a building. RIS can be installed on various surfaces, including building facades, highway polls, advertising panels, vehicle windows, pedestrian clothing, and so on [8]. Even though there is a blockage, the RIS introduces a virtual LoS between RSU and vehicles. As the building with RIS is appropriately far from the RSU and vehicles, RIS serves as a smart reflector. This results in a dual-hop channel. It is impractical to have accurate channel information at RIS due to a large number of vehicles and their high mobility. This implies blind
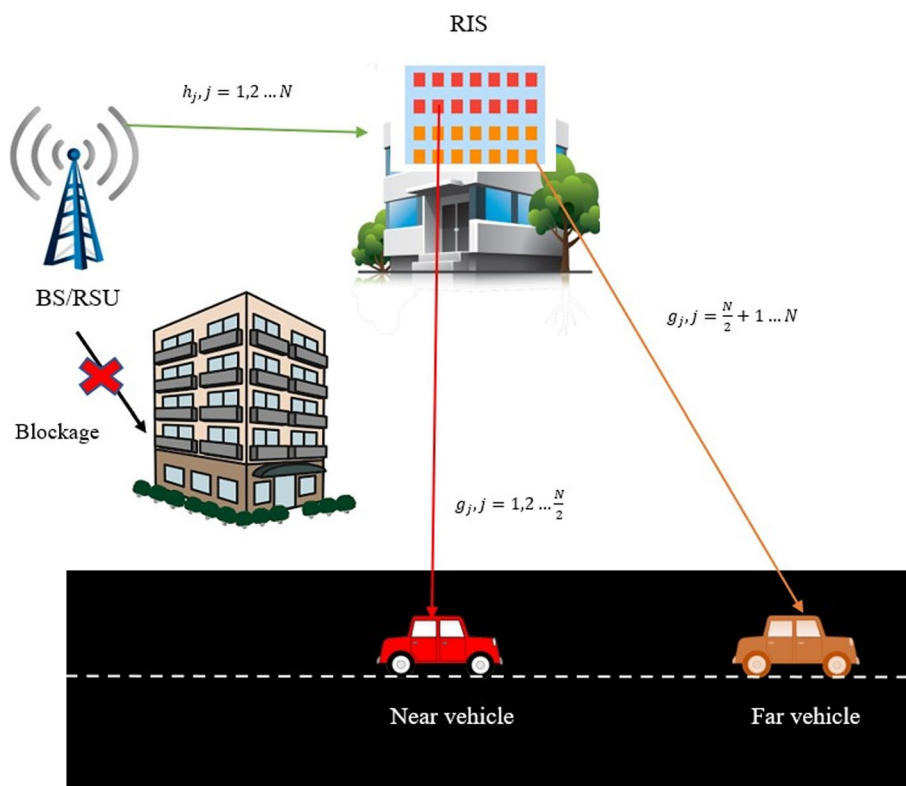

Fig. 3 Conceptual diagram of blind RIS-IR-FNOMA system for a downlink V2I scenario

transmission, in which the RIS elements introduce no phase shift. Due to the blind RIS configuration, only array gain is achieved based on the number of passive reflecting elements. However, no diversity gain is achieved.

In this proposed method, two vehicles are allotted with an equal number of reflecting elements. Single antenna is used at RSU, near and far vehicles. More power is allocated to the far vehicle than the near vehicle to meet QoS criteria. The order in which the vehicles' signals are decoded is fixed in FNOMA. The signal from the far vehicle is decoded first, with the signal from the near vehicle treated as interference. The far vehicle's signal is decoded at the near vehicle, and its impact is removed from the received signal via SIC. The near vehicle's signal is decoded from the residual signal.

A superposition-coded signal is generated at BS/RSU. It is given by

$$x_s = \sqrt{\beta_{\mathrm{nv}} P_s}\, x_{\mathrm{nv}} + \sqrt{\beta_{\mathrm{fv}} P_s}\, x_{\mathrm{fv}} \tag{1}$$

where β_{nv} and β_{fv} are the fraction of the total transmit power P_s allocated to near and far vehicles, respectively. x_{nv} and x_{fv} are the transmitted unit energy symbols corresponding to near and far vehicles, respectively. The power is allocated by BS/RSU to near and far vehicles such that the following constraint is met.

$$\beta_{\mathrm{nv}} + \beta_{\mathrm{fv}} = 1, \beta_{\mathrm{fv}} > \beta_{\mathrm{nv}} > 0 \tag{2}$$

The channel between the BS/RSU and the jth RIS element is $h_j = \alpha_j e^{-i\phi_j}$, $h_j \sim C\mathcal{N}(0,1)$, where α_j and ϕ_j are the magnitude and phase of h_j. The channel between jth RIS element and the vehicle is $g_j = \gamma_j e^{-i\psi_j}, g_j \sim C\mathcal{N}(0,1)$, where γ_j and ψ_j are the magnitude and phase of g_j. The number of reflecting elements assigned to the near and far vehicles are denoted by (N_{nv}) and (N_{fv}), respectively. Assuming that they are equal, the received signal at the far vehicle is given by

$$y_{\mathrm{fv}} = \underbrace{\left(\sum_{j=\frac{N}{2}+1}^{N} h_j g_j\right)}_{L} x_s + w_{\mathrm{fv}} \tag{3}$$

where w_{fv} is the additive white Gaussian noise at the far vehicle, which follows $C\mathcal{N}(0,N_o)$, N_o is the noise variance. In Eq. (3), L is the dual-hop channel effect corresponding to a far vehicle. According to the CLT, L follows a complex Gaussian distribution when the number of reflecting elements assigned to the far vehicle is greater than 16, i.e., $L \sim C\mathcal{N}(0,N_{\mathrm{fv}})$ [40]. By substituting (1) in (3), the received signal at far vehicle is rewritten as

$$y_{\mathrm{fv}} = L\,\sqrt{\beta_{\mathrm{nv}} P_s}\, x_{\mathrm{nv}} + L\,\sqrt{\beta_{\mathrm{fv}} P_s}\, x_{\mathrm{fv}} + w_{\mathrm{fv}} \tag{4}$$

In FNOMA, the near vehicle receives less power, while the far vehicle receives more power. The first term in (4) is not dominant over the second term because the cumulative dual-hop channel for the far vehicle is weaker and β_{nv} is smaller. As a result, the far vehicle's signal is detected by considering the near vehicle's signal as interference. The signal-to-interference plus noise ratio (SINR) for decoding a signal from a far vehicle while treating a signal from a near vehicle as interference is given by

$$\vartheta_{\text{fv}}^{x_{\text{fv}}} = \frac{|L|^2 \beta_{\text{fv}} \rho_s}{|L|^2 \beta_{\text{nv}} \rho_s + 1} \tag{5}$$

where $\rho_s = \frac{P_s}{N_0}$ is the transmit SNR. The outage occurs at the far vehicle when [18],

$$\log_2\left(1 + \vartheta_{\text{fv}}^{x_{\text{fv}}}\right) \leq \tilde{R}_{\text{fv}} \tag{6}$$

where $\tilde{R}_{\text{fv}}$ is the desired rate demand of the far vehicle. Substituting (5) in (6), it is rewritten as

$$\log_2\left(1 + \frac{|L|^2 \beta_{\text{fv}} \rho_s}{|L|^2 \beta_{\text{nv}} \rho_s + 1}\right) \leq \tilde{R}_{\text{fv}} \tag{7}$$

Let $R_{\text{fv}} = 2^{\tilde{R}_{\text{fv}}} - 1$ and $\eta_{\text{fv}} = |L|^2$, (7) is simplified as

$$\eta_{\text{fv}} \leq \underbrace{\frac{R_{\text{fv}}}{(\beta_{\text{fv}} - \beta_{\text{nv}} R_{\text{fv}}) \rho_s}}_{r_{\text{fv}}} \tag{8}$$

The comprehensive derivation of (8) is given in "Appendix 1." η_{fv} follows Chi-square distribution with two degrees of freedom. The corresponding mean of η_{fv} is $E\{\eta_{\text{fv}}\} = \delta_{\text{fv}}^2 N_{\text{fv}}$, where δ_{fv}^2 is the average channel gain of far vehicle. The probability density function (pdf) of η_{fv} is given by

$$f_{\eta_{\text{fv}}}^{(\eta_{\text{fv}})} = \frac{1}{\delta_{\text{fv}}^2 N_{\text{fv}}} e^{-\left(\frac{\eta_{\text{fv}}}{\delta_{\text{fv}}^2 N_{\text{fv}}}\right)}, \ \eta_{\text{fv}} \geq 0 \tag{9}$$

The outage probability for the far vehicle is calculated using

$$P_{\text{fv}}^o = \int_0^{r_{\text{fv}}} f_{\eta_{\text{fv}}}^{(\eta_{\text{fv}})} d\eta_{\text{fv}} \tag{10}$$

Substituting (9), the outage probability for the far vehilce is expressed as

$$P_{\text{fv}}^o = 1 - \exp\left\{-\left(\frac{R_{\text{fv}}}{(\beta_{\text{fv}} - \beta_{\text{nv}} R_{\text{fv}}) \delta_{\text{fv}}^2 N_{\text{fv}} \rho_s}\right)\right\} \tag{11}$$

The comprehensive derivation of (11) is given in "Appendix 2." The received signal at the near vehicle is given by

$$y_{\text{nv}} = \underbrace{\left(\sum_{j=1}^{\frac{N}{2}} h_j g_j\right)}_{M} x_s + w_{\text{nv}} \tag{12}$$

where w_{nv} is the additive white Gaussian noise at the near vehicle, which follows $\mathcal{CN}(0, N_o)$. M is the dual-hop channel effect corresponding to the near vehicle. According to the CLT, M follows a complex Gaussian distribution when the number of

reflecting elements assigned to the near vehicle is greater than 16, i.e., $M \sim \mathcal{CN}(0, N_{nv})$ [40]. By substituting (1) in (12), the received signal at the near vehicle is rewritten as

$$y_{nv} = M \sqrt{\beta_{nv} P_s} \, x_{nv} + M \sqrt{\beta_{fv} P_s} \, x_{fv} + w_{nv} \tag{13}$$

The second term in (13) is dominant over the first term, because both the value of M and β_{fv} are higher. As a result, the signal from the far vehicle is detected first by the near vehicle. The SINR of decoding a signal from a far vehicle at a near vehicle is given by

$$\vartheta_{nv}^{x_{fv}} = \frac{|M|^2 \beta_{fv} \rho_s}{|M|^2 \beta_{nv} \rho_s + 1} \tag{14}$$

After eliminating the influence of x_{fv} from y_{nv} using SIC, the received signal at the near vehicle is given by,

$$\tilde{y}_{nv} \approx M \sqrt{\beta_{nv} \rho_s} \, x_{nv} + w_{nv} \tag{15}$$

The signal of a near vehicle is detected using (15). The SNR for decoding x_{nv} at near vehicle is given by

$$\vartheta_{nv}^{x_{nv}} = |M|^2 \beta_{nv} \rho_s \tag{16}$$

The decoding of the far vehicle's signal fails at the near vehicle when [18]

$$\log_2\left(1 + \vartheta_{nv}^{x_{fv}}\right) \leq \tilde{R}_{fv} \tag{17}$$

By substituting (14) in (17),

$$\log_2\left(1 + \frac{|M|^2 \beta_{fv} \rho_s}{|M|^2 \beta_{nv} \rho_s + 1}\right) \leq \tilde{R}_{fv} \tag{18}$$

After simplification, (18) is written as,

$$|M|^2 \leq \frac{R_{fv}}{(\beta_{fv} - \beta_{nv} R_{fv}) \rho_s} \tag{19}$$

The comprehensive derivation of (19) is given in "Appendix 3." The decoding of the near vehicle's signal fails at the near vehicle when [18],

$$\log_2\left(1 + \vartheta_{nv}^{x_{nv}}\right) \leq \tilde{R}_{nv} \tag{20}$$

where $\tilde{R}_{nv}$ is the desired rate demand of the near vehicle. Substituting (16) in (20) gives

$$\log_2\left(1 + |M|^2 \beta_{nv} \rho_s\right) \leq \tilde{R}_{nv} \tag{21}$$

After simplification, (21) is written as,

$$|M|^2 \leq \frac{R_{nv}}{\beta_{nv} \rho_s} \tag{22}$$

where $R_{\text{nv}} = 2^{\tilde{R}_{\text{nv}}} - 1$. "Appendix 4" illustrates the comprehensive derivation of (22). As a result, the condition for which decoding of a near vehicle's signal fails at a near vehicle is provided by

$$\eta_{\text{nv}} = |M|^2 \leq \underbrace{\max \left\{ \frac{R_{\text{fv}}}{(\beta_{\text{fv}} - \beta_{\text{nv}}R_{\text{fv}})\rho_s}, \frac{R_{\text{nv}}}{\beta_{\text{nv}}\rho_s} \right\}}_{r_{\text{nv}}} \tag{23}$$

η_{nv} follows Chi-square distribution with two degrees of freedom. The corresponding mean is $E\{\eta_{\text{nv}}\} = \delta_{\text{nv}}^2 N_{\text{nv}}$, where δ_{nv}^2 is the average channel gain of near vehicle. The pdf of η_{nv} is given by

$$f_{\eta_{\text{nv}}}^{(\eta_{\text{nv}})} = \frac{1}{\delta_{\text{nv}}^2 N_{\text{nv}}} e^{-\left(\frac{\eta_{\text{nv}}}{\delta_{\text{nv}}^2 N_{\text{nv}}}\right)}, \quad \eta_{\text{nv}} \geq 0 \tag{24}$$

The outage probability of near vehicle is calculated using

$$P_{\text{nv}}^o = \int_0^{r_{\text{nv}}} f_{\eta_{\text{nv}}}^{(\eta_{\text{nv}})} \mathrm{d}\eta_{\text{nv}} \tag{25}$$

By substituting (24) in (25) and simplifying,

$$P_{\text{nv}}^o = 1 - \exp\left\{ -\frac{1}{\delta_{\text{nv}}^2 N_{\text{nv}}} \left(\max\left\{ \frac{R_{\text{fv}}}{(\beta_{\text{fv}} - \beta_{\text{nv}}R_{\text{fv}})\rho_s}, \frac{R_{\text{nv}}}{\beta_{\text{nv}}\rho_s} \right\} \right) \right\} \tag{26}$$

The comprehensive derivation of (26) is given in "Appendix 5." The throughput of blind RIS-IR-FNOMA is given by [41],

$$T = \tilde{R}_{\text{nv}} \left(1 - P_{\text{nv}}^o\right) + \tilde{R}_{\text{fv}} \left(1 - P_{\text{fv}}^o\right) \tag{27}$$

where P_{nv}^o and P_{fv}^o are given in (26) and (11), respectively.

2.2 Blind RIS-RSU-FNOMA

The conceptual diagram of the blind RIS-RSU-FNOMA system for a downlink V2I scenario is shown in Fig. 4. Enhanced performance is obtained when RIS is deployed in close proximity to the transmitter or receiver units [40, 42]. In Fig. 4, RIS with N reflecting elements is supposed to be near RSU. As a dedicated link is used to connect the RSU and RIS, the RSU-RIS channel is deterministic, and its fading effect is minimal. As a result, communication between the RIS-RSU and the vehicles is limited to a single hop. In this section, closed-form analytical outage probability and throughput expressions are derived for blind RIS-RSU-FNOMA. The received signal at the far vehicle is given by

$$y_{\text{fv}} = \underbrace{\left(\sum_{j=\frac{N}{2}+1}^{N} g_j \right)}_{H} x_s + w_{\text{fv}} \tag{28}$$
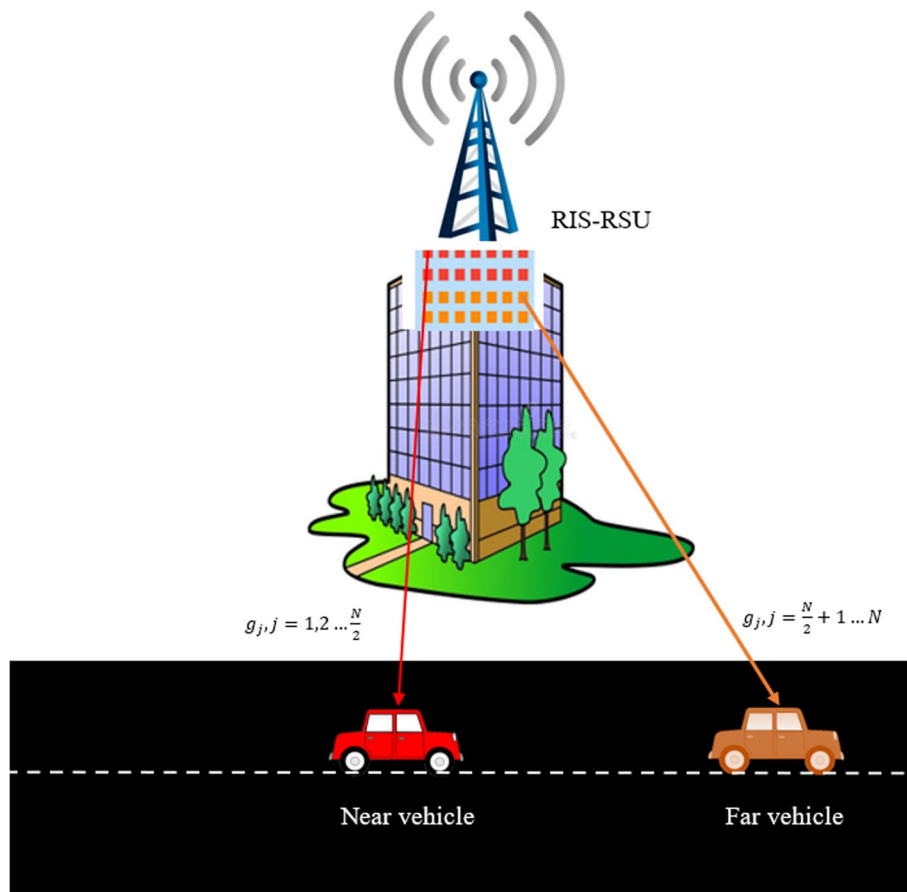
Fig. 4 Conceptual diagram of blind RIS-RSU-FNOMA system for a downlink V2I scenario

In (28), H is the cumulative channel effect corresponding to the far vehicle, and it follows complex Gaussian distribution based on CLT, i.e., $H \sim \mathcal{CN}(0, N_{\mathrm{fv}})$. By substituting (1) in (28), the received signal at the far user is rewritten as

$$y_{\mathrm{fv}} = H \sqrt{\beta_{\mathrm{nv}} P_s}\, x_{\mathrm{nv}} + H \sqrt{\beta_{\mathrm{fv}} P_s}\, x_{\mathrm{fv}} + w_{\mathrm{fv}} \tag{29}$$

As per the concept of FNOMA, power is allocated for near and far vehicles in RIS-RSU-FNOMA system. The first term in (29) is not dominant over the second term because the cumulative channel for the far vehicle is weaker and β_{nv} is smaller. As a result, the far vehicle's signal is detected by considering the near vehicle's signal as interference. The SINR for decoding a signal from a far vehicle while treating a signal from a near vehicle as interference is given by

$$\vartheta_{\mathrm{fv}}^{x_{\mathrm{fv}}} = \frac{|H|^2 \beta_{\mathrm{fv}} \rho_s}{|H|^2 \beta_{\mathrm{nv}} \rho_s + 1} \tag{30}$$

The outage occurs at far vehicle when condition in (6) is met [18]. Let $\rho_{\mathrm{fv}} = |H|^2$, the condition for the outage of the far vehicle is given by

Kumaravelu *et al. J Wireless Com Network* (2023) 2023:83

Page 13 of 25

$$\rho_{fv} \leq \underbrace{\frac{R_{fv}}{(\beta_{fv} - \beta_{nv}R_{fv})\rho_s}}_{r_{fv}} \tag{31}$$

ρ_{fv} follows Chi-square distribution with two degrees of freedom. The corresponding mean of ρ_{fv} is $E\{\rho_{fv}\} = \kappa_{fv}^2 N_{fv}$, where κ_{fv}^2 is the average channel gain of far vehicle. The pdf of ρ_{fv} can be written similar to (9). Using the expression similar to (10), the probability of outage for the far vehicle is obtained as

$$P_{fv}^o = 1 - \exp\left\{ -\left(\frac{R_{fv}}{(\beta_{fv} - \beta_{nv}R_{fv})\kappa_{fv}^2 N_{fv}\rho_s} \right) \right\} \tag{32}$$

The received signal at the near vehicle is given by

$$y_{nv} = \underbrace{\left(\sum_{j=1}^{\frac{N}{2}} g_j \right)}_{G} x_s + w_{nv} \tag{33}$$

where G is the cumulative channel effect corresponding to the near vehicle, and it follows complex Gaussian distribution based on CLT, i.e., $G \sim \mathcal{CN}(0, N_{nv})$. By substituting (1) in (33), the received signal at the near user is rewritten as

$$y_{nv} = G \sqrt{\beta_{nv}P_s}\, x_{nv} + G \sqrt{\beta_{fv}P_s}\, x_{fv} + w_{nv} \tag{34}$$

The second term in (34) is dominant over the first term, because G and β_{fv} are higher. As a result, the signal from the far vehicle is detected first by the near vehicle. The SINR of decoding a signal from a far vehicle at a near vehicle is given by

$$\vartheta_{nv}^{x_{fv}} = \frac{|G|^2 \beta_{fv}\rho_s}{|G|^2 \beta_{nv}\rho_s + 1} \tag{35}$$

The influence of x_{fv} is eliminated from y_{nv} using SIC after it has been decoded.

$$\tilde{y}_{nv} \approx G\sqrt{\beta_{nv}\rho_s}\, x_{nv} + w_{nv} \tag{36}$$

The signal of a nearby vehicle is then detected. The SNR for decoding x_{nv} at near vehicle is

$$\vartheta_{nv}^{x_{nv}} = |G|^2 \beta_{nv}\rho_s \tag{37}$$

The decoding of the far vehicle's signal fails at the near vehicle when the condition in (17) is met. By substituting (35) in (17), the condition is given by

$$|G|^2 \leq \frac{R_{fv}}{(\beta_{fv} - \beta_{nv}R_{fv})\rho_s} \tag{38}$$

The decoding of a near vehicle's signal fails at a near vehicle when the condition in (20) is met. By substituting (37) in (20), the condition is given by

$$|G|^2 \leq \frac{R_{\mathrm{nv}}}{\beta_{\mathrm{nv}}\rho_s} \tag{39}$$

The condition for which decoding of a near vehicle's signal fails at the near vehicle is provided by

$$\rho_{\mathrm{nv}} = |G|^2 \leq \underbrace{\max\left\{\frac{R_{\mathrm{fv}}}{(\beta_{\mathrm{fv}} - \beta_{\mathrm{nv}}R_{\mathrm{fv}})\rho_s}, \frac{R_{\mathrm{nv}}}{\beta_{\mathrm{nv}}\rho_s}\right\}}_{r_{\mathrm{nv}}} \tag{40}$$

ρ_{nv} follows Chi-square distribution with two degrees of freedom. The corresponding mean is $E\{\rho_{\mathrm{nv}}\} = \kappa_{\mathrm{nv}}^2 N_{\mathrm{nv}}$, where κ_{nv}^2 is the average channel gain of near vehicle. The outage probability at near vehicle is obtained as

$$P_{\mathrm{nv}}^o = 1 - \exp\left\{-\frac{1}{\kappa_{\mathrm{nv}}^2 N_{\mathrm{nv}}}\left(\max\left\{\frac{R_{\mathrm{fv}}}{(\beta_{\mathrm{fv}} - \beta_{\mathrm{nv}}R_{\mathrm{fv}})\rho_s}, \frac{R_{\mathrm{nv}}}{\beta_{\mathrm{nv}}\rho_s}\right\}\right)\right\} \tag{41}$$

The throughput of blind RIS-RSU-FNOMA is computed by using (27). Here, P_{nv}^o and P_{fv}^o are given in (41) and (32), respectively.

3 Results and discussion

In this section, the outage and throughput performances of blind RIS-IR-FNOMA and blind RIS-RSU-FNOMA are validated through simulation results. The simulation setup is given in Table 1. The parameters for the simulation study are chosen based on previous works [18, 29, 30, 38, 39]. The Monte Carlo simulation results are averaged over 10^6 random channel realizations. The outage probability performance of the RIS-IR-FNOMA far vehicle is compared for different numbers of RIS elements in Fig. 5. The simulated outage closely matched closed-form analytical curves produced by (11) for greater values of N. $N = 32$, $N = 64$, $N = 128$ and $N = 256$ systems require SNR of ≈ 29 dB, ≈ 26 dB, ≈ 23 dB, and ≈ 20 dB, respectively, to achieve the required outage

Table 1 Parameters for simulation study [18, 29, 30, 38, 39]

| Parameter	Typical value
Block size	10^6
Desired data rate demand of far vehicle $\left(\tilde{R}_{\mathrm{fv}}\right)$	1 b/s/Hz
Desired data rate demand of near vehicle $\left(\tilde{R}_{\mathrm{nv}}\right)$	1 b/s/Hz
Number of reflecting elements (N)	32, 64, 128, 256, 512
Number of users	2
Average channel gain of far vehicle	1
Average channel gain of near vehicle	3
Power fraction allocated to near vehicle (β_{nv})	0.1
Power fraction allocated to far vehicle (β_{fv})	0.9
Target outage probability for analysis	10^{-4}
Target throughput (b/s/Hz)	2 b/s/Hz
Bandwidth	1 GHz
Noise variance (σ^2)	-174 dBm
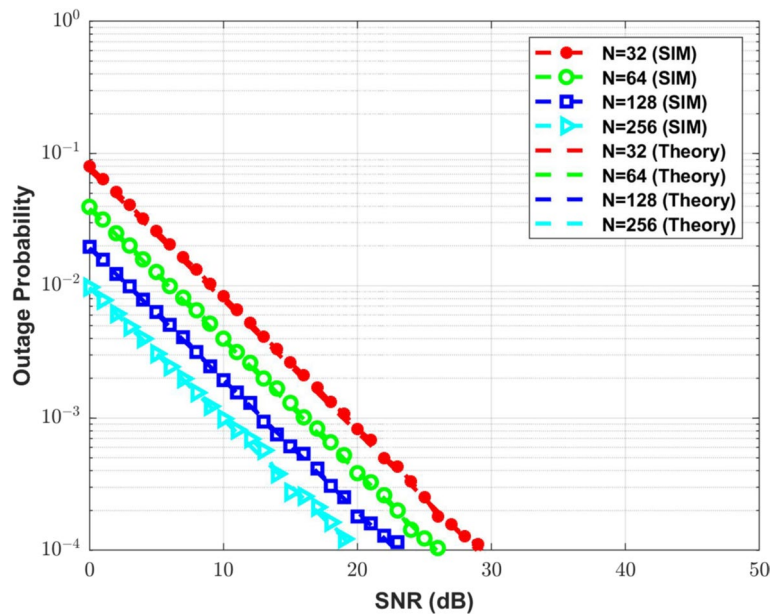
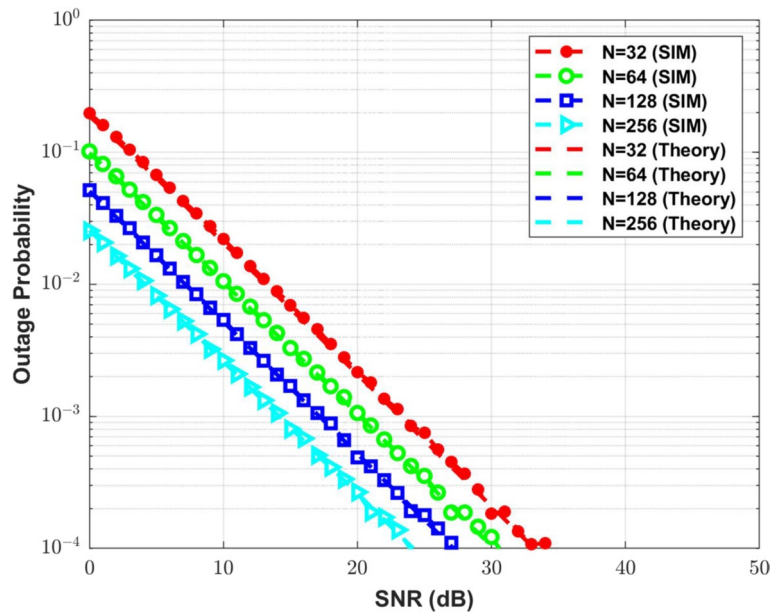**Fig. 5** Outage probability comparison of RIS-IR-FNOMA far vehicle for various N

Fig. 6 Outage probability comparison of RIS-IR-FNOMA near vehicle for various N

probability of 10^{-4}. The SNR requirement is found to be reduced by ≈ 3 dB when the number of reflecting elements is doubled.

The outage probability performance of RIS-IR-FNOMA near vehicle for various numbers of RIS elements is compared in Fig. 6. The simulated outage resembled the closed-form mathematical curves resulting from (26), especially for higher values of N. $N = 32$, $N = 64$, $N = 128$ and $N = 256$ systems require SNR of ≈ 33 dB, ≈ 30 dB, ≈ 27 dB, and

Kumaravelu *et al. J Wireless Com Network*   (2023) 2023:83

Page 16 of 25

≈ 24 dB, respectively, to achieve a target outage probability of 10^{-4}. It has been noted that increasing the number of reflecting elements by twofold lowers the SNR required by ≈ 3 dB. From Figs. 5 and 6, it is observed that the far vehicle's outage performance is superior to the near vehicle's because the far vehicle is supplied more power.

In Fig. 7, the throughput (b/s/Hz) performance of blind RIS-IR-FNOMA is compared for different numbers of RIS elements and $\widetilde{R}_{nv} = \widetilde{R}_{fv} = 1$ b/s/Hz. The throughput curves are plotted based on the expression in (27). The throughput of RIS-IR-FNOMA system is increased by increasing transmit power at RSU. At about ≈ 0 dB, the sum throughput of blind RIS-IR-FNOMA with $N = 512$ reaches 2 b/s/Hz. Blind RIS-IR-FNOMA, for example, with $N = 32$ reflecting elements, achieves a maximum throughput of 2 b/s/Hz at ≈ 15 dB. It is also been noted that the increase in N decreases the SNR requirement to reach the target throughput. It is also obvious that the Monte Carlo simulation curves for blind RIS-IR-FNOMA system closely match closed-form analytical curves.

The outage probability of RIS-RSU-FNOMA far vehicle for varying N is shown in Fig. 8. For $N = 32$, $N = 64$, $N = 128$ and $N = 256$ reflecting elements, the far vehicle attains an outage probability of 10^{-4} at ≈ 29 dB, ≈ 26 dB, ≈ 23 dB, ≈ 20 dB. The SNR gain grows as N increases. Based on the outage expression in (32), analytical curves for various N are obtained. For all N, there is a close match between the Monte Carlo simulation curves and the analytical curves. The outage probability of the RIS-RSU-FNOMA near vehicle for varying N is shown in Fig. 9. The analytical curves for various N are drawn based on the outage expression in (41). When comparing Figs. 8 and 9, it is evident that the far vehicle's outage performance is better to the near vehicle's. Figure 9's other trends follow Fig. 8. In Fig. 10, the throughput (b/s/Hz) performance of blind RIS-RSU-FNOMA is compared for different numbers of RIS elements and $\widetilde{R}_{nv} = \widetilde{R}_{fv} = 1$ b/s/Hz. Figure 7's explanations are applicable to Fig. 10.
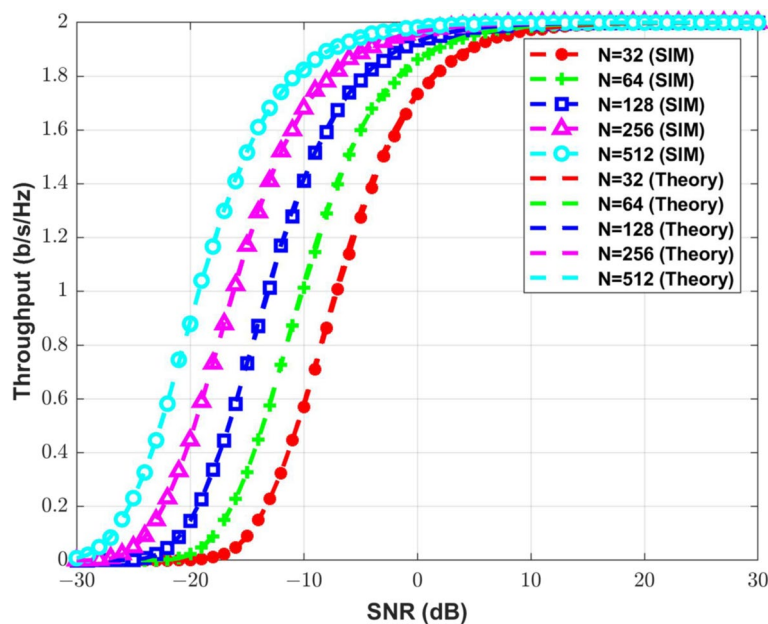

Fig. 7 Throughput comparison of RIS-IR-FNOMA for various N and $\widetilde{R}_{fv} = \widetilde{R}_{nv} = 1$ b/s/Hz

Kumaravelu *et al. J Wireless Com Network*   (2023) 2023:83
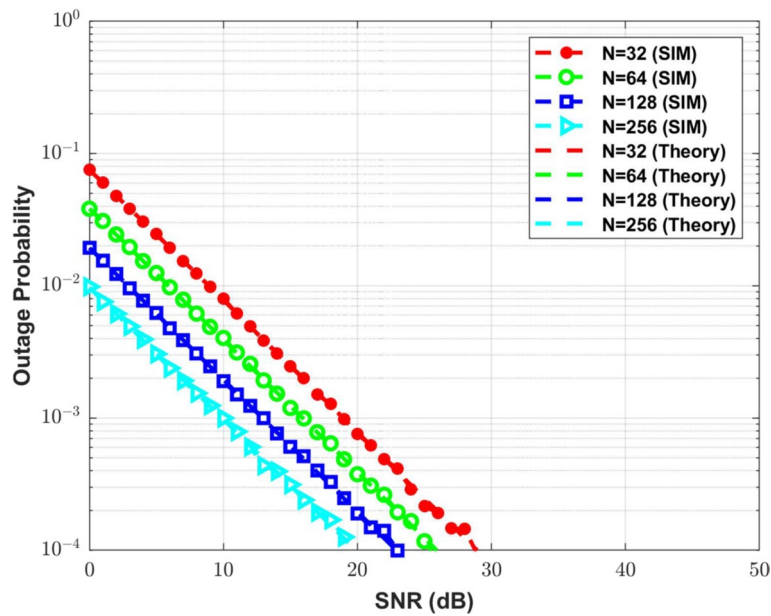
Page 17 of 25

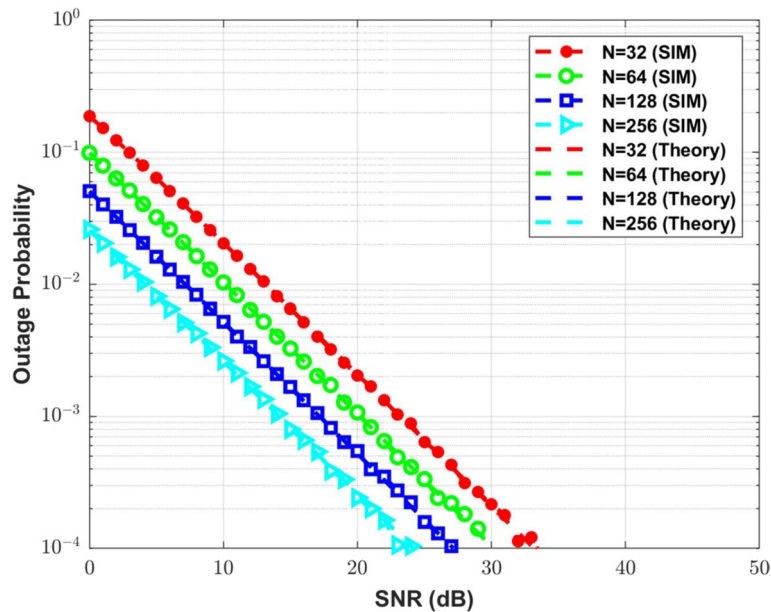**Fig. 8** Outage probability comparison of RIS-RSU-FNOMA far vehicle for various *N*

Fig. 9 Outage probability comparison of RIS-RSU-FNOMA near vehicle for various *N*

To demonstrate the efficacy of the suggested RIS-aided approaches, comparisons are made with classic time division multiple access (TDMA), FNOMA [18], ONOMA [18], CNOMA [29], and SWIPT-CNOMA [30]. $N = 64$ reflective elements are assumed in the RIS. The probability of outage attained by the far vehicle using various systems is shown in Fig. 11. The outage probability of far vehicle for OMA (TDMA), FNOMA, ONOMA, CNOMA, and SWIPT-NOMA is given by
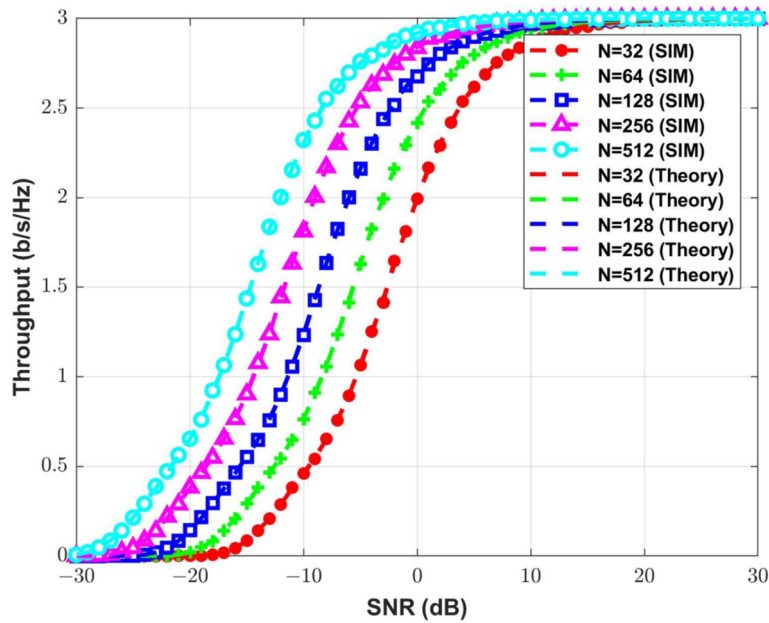
Fig. 10 Throughput comparison of RIS-RSU-FNOMA for various N and $\widetilde{R}_{\mathrm{fv}} = \widetilde{R}_{\mathrm{nv}} = 1$ b/s/Hz
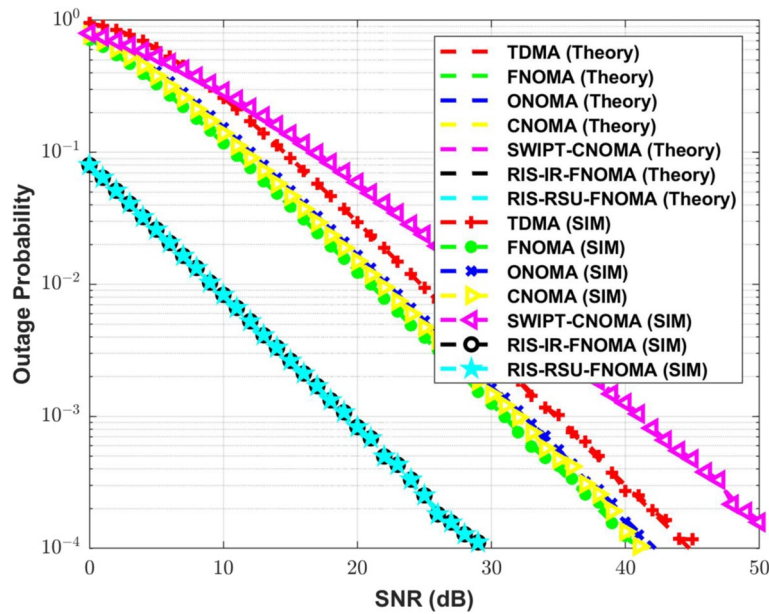

Fig. 11 Far vehicle's outage probability comparison for different methods

$$P_{\mathrm{fv}}^{\mathrm{o\text{-}OMA}} = 1 - \exp\left(-\frac{c_{\mathrm{fv}}}{\rho_s \delta_{\mathrm{fv}}^2}\right) \tag{42}$$

where $c_{\mathrm{fv}} = 2^{2\widetilde{R}_{\mathrm{fv}}} - 1$.

$$P_{\text{fv}}^{\text{o-FNOMA}} = 1 - \exp\left\{-\left(\frac{R_{\text{fv}}}{(\beta_{\text{fv}} - \beta_{\text{nv}}R_{\text{fv}})\delta_{\text{fv}}^2\rho_s}\right)\right\} \tag{43}$$

$$P_{\text{fv}}^{\text{o-ONOMA}} = 1 - \exp\left\{-\left(\frac{R_{\text{fv}}}{(\beta_{\text{fv}} - \beta_{\text{nv}}R_{\text{fv}})\delta_H^2\rho_s}\right)\right\} \tag{44}$$

where $\frac{1}{\delta_H^2} = \frac{1}{\delta_{\text{fv}}^2} + \frac{1}{\delta_{\text{nv}}^2}$

$$P_{\text{fv}}^{\text{o-CNOMA}} = \min\left\{1 - \exp\left(-\frac{c_{\text{fv}}}{\rho_s\delta_{\text{fv}}^2(\beta_{\text{fv}} - \beta_{\text{nv}}c_{\text{fv}})}\right), 1 - \exp\left(-\frac{c_{\text{fv}}}{\rho_s\delta_{\text{nf}}^2}\right)\right\} \tag{45}$$

where δ_{nf}^2 is the average gain of channel between near and far vehicle.

$$P_{\text{fv}}^{\text{o-SWIPT-CNOMA}} = 1 - \exp\left(-\frac{c_{\text{fv}}\sigma^2}{P_H\delta_{\text{nf}}^2}\right) \tag{46}$$

where σ^2 is the variance of noise and P_H is the harvested energy during direct transmission. The outage probability of near vehicle for OMA (TDMA), FNOMA, ONOMA, CNOMA, and SWIPT-NOMA is given by

$$P_{\text{nv}}^{\text{o-OMA}} = 1 - \exp\left(-\frac{c_{\text{nv}}}{\rho_s\delta_{\text{nv}}^2}\right) \tag{47}$$

where $c_{\text{nv}} = 2^{2\widetilde{R}_{\text{nv}}} - 1$.

$$P_{\text{nv}}^{\text{o-FNOMA}} = 1 - \exp\left\{-\frac{1}{\delta_{\text{nv}}^2}\left(\max\left\{\frac{R_{\text{fv}}}{(\beta_{\text{fv}} - \beta_{\text{nv}}R_{\text{fv}})\rho_s}, \frac{R_{\text{nv}}}{\beta_{\text{nv}}\rho_s}\right\}\right)\right\} \tag{48}$$

$$P_{\text{nv}}^{\text{o-ONOMA}} = 1 - \exp\left(-\frac{\varphi}{\delta_{\text{fv}}^2}\right) - \exp\left(-\frac{\varphi}{\delta_{\text{nv}}^2}\right) + \exp\left(-\frac{\varphi}{\delta_H^2}\right) \tag{49}$$

where $\varphi = \max\left\{\frac{R_{\text{fv}}}{(\beta_{\text{fv}} - \beta_{\text{nv}}R_{\text{fv}})\rho_s}, \frac{R_{\text{nv}}}{\beta_{\text{nv}}\rho_s}\right\}$.

$$P_{\text{nv}}^{\text{o-CNOMA}} = 1 - \exp\left(-\frac{1}{\delta_{\text{nv}}^2}\max\left\{\frac{c_{\text{fv}}}{(\beta_{\text{fv}} - \beta_{\text{nv}}c_{\text{fv}})\rho_s}, \frac{c_{\text{nv}}}{\beta_{\text{nv}}\rho_s}\right\}\right) \tag{50}$$

$$P_{\text{nv}}^{\text{o-SWIPT-CNOMA}} = 1 - \exp\left(-\frac{1}{\delta_{\text{nv}}^2}\max\left\{\frac{c_{\text{fv}}}{(\beta_{\text{fv}} - \beta_{\text{nv}}c_{\text{fv}})(1 - \psi)\rho_s}, \frac{c_{\text{nv}}}{(1 - \psi)\beta_{\text{nv}}\rho_s}\right\}\right) \tag{51}$$

where ψ is the fraction for energy harvesting. To simulate SWIPT-CNOMA system, $\delta_{\text{nf}}^2 = 2$, $\psi = 0.5$ and efficiency of energy harvesting circuit $\eta_{\text{eff}} = 0.7$ are considered. The increase in transmit power at RSU improves the outage performance of all the systems. Both proposed RIS-aided FNOMA systems (IR and RSU) perform nearly equally well and reach the desired outage probability of 10^{-4} at ≈ 29 dB. FNOMA and CNOMA systems outperform other NOMA variants due to their higher power allocation and selection diversity. Because of the constraints on resources, TDMA performs poorly.

SWIPT-NOMA's performance is subpar compared to other systems due to constraints on resources and fractional harvested power used for relaying. The suggested RIS-aided FNOMA systems outperform TDMA, FNOMA, ONOMA, CNOMA, and SWIPT-CNOMA systems by ≈ 16 dB, ≈ 11 dB, ≈ 13 dB, ≈ 12 dB, and ≈ 23 dB, respectively.

The probability of outage achieved by the near vehicle using various methods is compared in Fig. 12. It is obvious that the suggested RIS-aided system performs better than all previous systems, particularly up to ≈ 25 dB SNR. After ≈ 25 dB, ONOMA performs better since user channel gains determine the order of decoding. Here, $N = 64$ is used by the RIS-aided systems. Increasing the number of RIS elements improves the performance of the RIS-aided system over other systems. Due to very lower power allocation, FNOMA performs poor than ONOMA. When compared to all other systems, CNOMA and SWIPT-CNOMA perform the worst due to time resource constraints. The recommended RIS-aided FNOMA systems outperform TDMA, FNOMA, CNOMA, and SWIPT-CNOMA systems by ≈ 9 dB, ≈ 14 dB, ≈ 20 dB, and ≈ 25 dB, respectively. In comparison with other OMA and NOMA variants, the outage probability of far and near vehicles is relatively low for blind RIS-assisted schemes in high SNR regions. As the SNR increases, the gain of blind RIS-assisted methods becomes substantially higher.

The throughput attained by various systems is compared in Fig. 13. At ≈ 10 dB SNR, the RIS-assisted systems achieve the target throughput of 2 b/s/Hz. ONOMA, FNOMA, and TDMA systems achieve the desired throughput by ≈ 25 dB, ≈ 29 dB, and ≈ 29 dB, respectively. Even at 30 dB SNR, desired throughput is not achieved with CNOMA and SWIPT-CNOMA. Even though the ONOMA near vehicle outperforms the suggested RIS-aided systems with $N = 64$ in terms of outage probability, the proposed systems exhibit a ≈ 15 dB SNR gain in terms of throughput over ONOMA system.
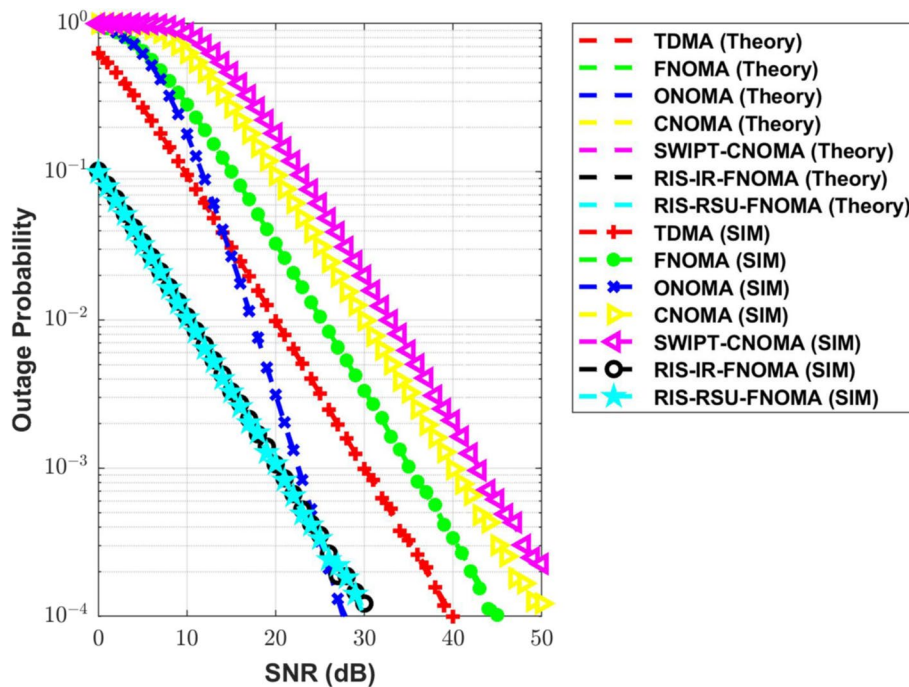

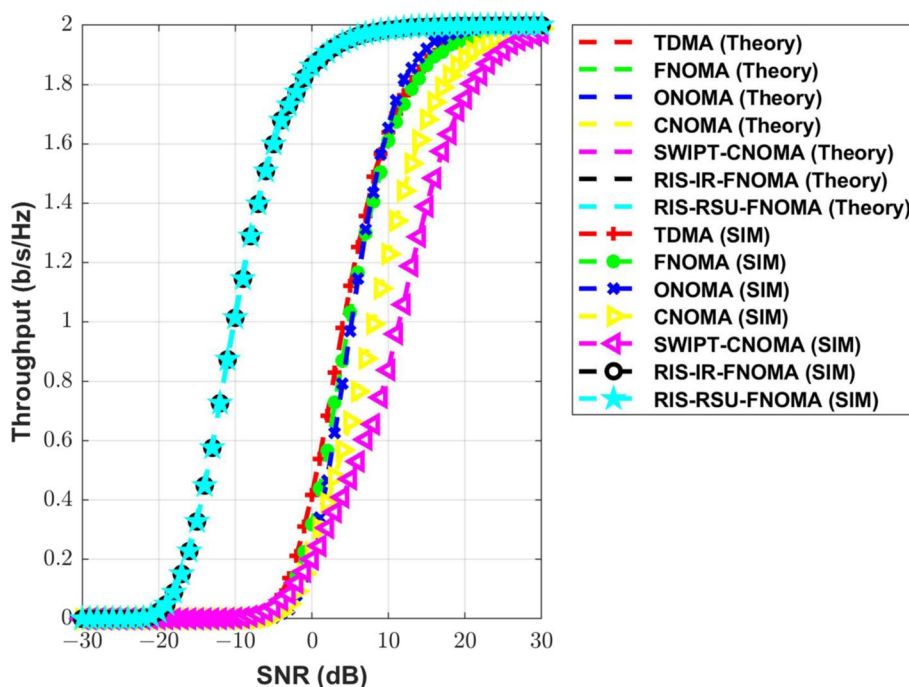**Fig. 12** Near vehicle's outage probability comparison for different methods

Fig. 13 Throughput comparison for different methods

4 Conclusions

This paper has presented the blind RIS-IR-FNOMA and RIS-RSU-FNOMA systems' closed-form analytical outage probability and throughput expressions for downlink V2I scenarios. The analytical and Monte Carlo simulation curves are almost identical. To guarantee QoS fairness, FNOMA gives far vehicles more power than nearby vehicles. As a result, for both blind RIS-IR-FNOMA and RIS-RSU-FNOMA systems, the far vehicle's outage performance is better than the near vehicle's. As the number of reflecting elements grows, so does the outage and throughput performance. The blind RIS-IR-FNOMA and RIS-RSU-FNOMA systems outperform the OMA and NOMA variants in terms of outage probability and throughput. RIS-assisted FNOMA is better than NOMA variants for vehicular environments because of its massive connectivity, stronger reliability, and ability to give improved outage and throughput even without channel knowledge. As RIS-RSU-FNOMA system performs identically to RIS-IR-FNOMA system in terms of throughput and outage performance and more realistic in practical circumstances, it could be a viable contender for vehicular applications.

Blind RIS can be substituted with discrete phase shifter-assisted RIS in the future, and its usefulness in vehicular environments can be studied. Random power allocations for FNOMA are performed in the suggested study, which could be changed to achieve optimal power allocation. The proposed systems can be tested with multiple vehicles by considering user pairing. The performance of far vehicles can be improved further by employing a CNOMA system, in which cooperative combining is performed at the far vehicle. The proposed RIS-aided system can be modified with CNOMA in the future, and its performance for uplink and downlink transmissions can be tested.

Kumaravelu *et al. J Wireless Com Network*   (2023) 2023:83

Page 22 of 25

Appendices

Appendix 1. Condition for outage at far vehicle

Taking antilog on both sides of (7)

$$1 + \frac{|L|^2 \beta_{\text{fv}} \rho_s}{|L|^2 \beta_{\text{nv}} \rho_s + 1} \leq 2^{\widetilde{R}_{\text{fv}}} \tag{52}$$

$$\frac{|L|^2 \beta_{\text{fv}} \rho_s}{|L|^2 \beta_{\text{nv}} \rho_s + 1} \leq \underbrace{2^{\widetilde{R}_{\text{fv}}} - 1}_{R_{\text{fv}}} \tag{53}$$

$$|L|^2 \beta_{\text{fv}} \rho_s \leq R_{\text{fv}} + R_{\text{fv}} |L|^2 \beta_{\text{nv}} \rho_s \tag{54}$$

$$|L|^2 \rho_s (\beta_{\text{fv}} - \beta_{\text{nv}} R_{\text{fv}}) \leq R_{\text{fv}} \tag{55}$$

Simplifying this results in expression (8).

Appendix 2. Probability of outage expression for far vehicle

Substituting (9) in (10)

$$P_{\text{fv}}^o = \frac{1}{\delta_{\text{fv}}^2 N_{\text{fv}}} \int_0^{r_{\text{fv}}} e^{-\left(\frac{\eta_{\text{fv}}}{\delta_{\text{fv}}^2 N_{\text{fv}}}\right)} \, d\eta_{\text{fv}} \tag{56}$$

$$P_{\text{fv}}^o = \frac{1}{\delta_{\text{fv}}^2 N_{\text{fv}}} \left. \frac{e^{-\left(\frac{\eta_{\text{fv}}}{\delta_{\text{fv}}^2 N_{\text{fv}}}\right)}}{-\frac{1}{\delta_{\text{fv}}^2 N_{\text{fv}}}} \right|_0^{r_{\text{fv}}} \tag{57}$$

$$P_{\text{fv}}^o = \left[1 - \exp\left(\frac{-r_{\text{fv}}}{\delta_{\text{fv}}^2 N_{\text{fv}}}\right) \right] \tag{58}$$

Substituting r_{fv} results in expression (11).

Appendix 3. Condition for decoding of the far vehicle's signal fails at the near vehicle

Taking antilog on both sides of (18)

$$1 + \frac{|M|^2 \beta_{\text{fv}} \rho_s}{|M|^2 \beta_{\text{nv}} \rho_s + 1} \leq 2^{\widetilde{R}_{\text{fv}}} \tag{59}$$

$$\frac{|M|^2 \beta_{\text{fv}} \rho_s}{|M|^2 \beta_{\text{nv}} \rho_s + 1} \leq \underbrace{2^{\widetilde{R}_{\text{fv}}} - 1}_{R_{\text{fv}}} \tag{60}$$

$$|M|^2 \beta_{\text{fv}} \rho_s \leq R_{\text{fv}} + R_{\text{fv}} |M|^2 \beta_{\text{nv}} \rho_s \tag{61}$$

Kumaravelu *et al. J Wireless Com Network*   (2023) 2023:83

Page 23 of 25

$$|M|^2 \rho_s (\beta_{\text{fv}} - \beta_{\text{nv}} R_{\text{fv}}) \leq R_{\text{fv}} \tag{62}$$

Simplifying this results in expression (19).

Appendix 4. Condition for decoding of the near vehicle's signal fails at the near vehicle

Taking antilog on both sides of (21)

$$1 + |M|^2 \beta_{\text{nv}} \rho_s \leq 2^{\widetilde{R}_{\text{nv}}} \tag{63}$$

$$|M|^2 \beta_{\text{nv}} \rho_s \leq \underbrace{2^{\widetilde{R}_{\text{nv}}} - 1}_{R_{\text{nv}}} \tag{64}$$

$$|M|^2 \leq \frac{R_{\text{nv}}}{\beta_{\text{nv}} \rho_s} \tag{65}$$

Appendix 5. Probability of outage expression for near vehicle

Substituting (24) in (25)

$$P_{\text{nv}}^o = \frac{1}{\delta_{\text{nv}}^2 N_{\text{nv}}} \int_0^{r_{\text{nv}}} e^{-\left(\frac{\eta_{\text{nv}}}{\delta_{\text{nv}}^2 N_{\text{nv}}}\right)} \mathrm{d}\eta_{\text{nv}} \tag{66}$$

$$P_{\text{nv}}^o = \frac{1}{\delta_{\text{nv}}^2 N_{\text{nv}}} \left. \frac{e^{-\left(\frac{\eta_{\text{nv}}}{\delta_{\text{nv}}^2 N_{\text{nv}}}\right)}}{-\frac{1}{\delta_{\text{nv}}^2 N_{\text{nv}}}} \right|_0^{r_{\text{nv}}} \tag{67}$$

$$P_{\text{nv}}^o = \left[1 - \exp\left(\frac{-r_{\text{nv}}}{\delta_{\text{nv}}^2 N_{\text{nv}}}\right) \right] \tag{68}$$

Substituting r_{nv} results in expression (26).

Abbreviations

AP	Access point
BS	Base station
CLT	Central limit theorem
FNOMA	Fixed NOMA
IR	Intelligent reflector
ITS	Intelligent transportation system
MIMO	Multiple input–multiple output
NOMA	Non-orthogonal multiple access
OMA	Orthogonal multiple access
PLS	Physical layer security
QoS	Quality of service
RIS	Reconfigurable intelligent surfaces
RSU	Roadside unit
SNR	Signal-to-noise ratio
6G	Sixth-generation
SIC	Successive interference cancellation
3GPP	Third-generation partnership project
V2X	Vehicle-to-everything

V2I   Vehicle-to-infrastructure
V2V   Vehicle-to-vehicle
VANET   Vehicular ad hoc network

Declarations

Ethics approval and consent to participate
Not applicable

Consent for publication
The corresponding authors and with co-authors give our consent for the publication of identifiable details, which can include images and/or details within the text to be published in this Journal and Article.

Competing interests
All authors certify that they have no affiliations with or involvement in any organization or entity with any financial interest or non-financial interest in the subject matter or materials discussed in this manuscript.

References

1. E. Wagner, R.G. Atkins, A. Berning, A. Robbins, C. Watson, J. Anderle, et al., Examination of the traffic safety environment during the second quarter of 2020: Special report. Technical report, United States. National Highway Traffic Safety Administration. Office of Behavioral Safety Research (2020)
2. S. Declaration, in *Third Global Ministerial Conference on Road Safety: Achieving Global Goals 2030* (World Health Organization, Geneva, 2020)
3. X. Liu, B.S. Amour, A. Jaekel, A reinforcement learning-based congestion control approach for V2V communication in VANET. Appl. Sci. **13**(6), 3640 (2023)
4. C.S. Evangeline, V.B. Kumaravelu, A two-phase fuzzy based access network selection scheme for vehicular ad hoc networks. Peer-to-Peer Netw. Appl. **15**(1), 107–133 (2022)
5. H. Hasluda, Y. Kawamoto, N. Kato, Intelligent reflecting surface placement optimization in air–ground communication networks toward 6G. IEEE Wirel. Commun. **27**(6), 146–151 (2020)
6. A.U. Makarfi, K.M. Rabie, O. Kaiwartya, K. Adhikari, X. Li, M. Quiroz-Castellanos, R. Kharel, Reconfigurable intelligent surfaces-enabled vehicular networks: a physical layer security perspective (2020). arXiv preprint arXiv:2004.11288
7. J. Wang, W. Zhang, X. Bao, T. Song, C. Pan, Outage analysis for intelligent reflecting surface assisted vehicular communication networks, in *GLOBECOM 2020-2020 IEEE Global Communications Conference* (IEEE, 2020), pp. 1–6
8. Y. Liu, X. Liu, X. Mu, T. Hou, J. Xu, M. Di Renzo, N. Al-Dhahir, Reconfigurable intelligent surfaces: principles and opportunities. IEEE Commun. Surv. Tutor. **23**(3), 1546–1577 (2021)
9. C. Huang, S. Hu, G.C. Alexandropoulos, A. Zappone, C. Yuen, R. Zhang, M. Di Renzo, M. Debbah, Holographic MIMO surfaces for 6g wireless networks: opportunities, challenges, and trends. IEEE Wirel. Commun. **27**(5), 118–125 (2020)
10. E. Basar, Reconfigurable intelligent surfaces for doppler effect and multipath fading mitigation. Front. Commun. Netw. **14**, 672857 (2021)
11. E. Björnson, Ö. Özdogan, E.G. Larsson, Reconfigurable intelligent surfaces: three myths and two critical questions. IEEE Commun. Mag. **58**(12), 90–96 (2020)
12. E. Björnson, H. Wymeersch, B. Matthiesen, P. Popovski, L. Sanguinetti, E. de Carvalho, Reconfigurable intelligent surfaces: a signal processing perspective with wireless applications. IEEE Signal Process. Mag. **39**(2), 135–158 (2022)
13. P.G.S. Velmurugan, S.J. Thiruvengadam, V.B. Kumaravelu, S. Rajendran, R. Parameswaran, A.L. Imoize, Performance analysis of full duplex bidirectional machine type communication system using IRS with discrete phase shifter. Appl. Sci. **13**(12), 7128 (2023)
14. Y. Zhu, B. Mao, N. Kato, Intelligent reflecting surface in 6G vehicular communications: a survey. IEEE Open J. Veh. Technol. **3**, 266–277 (2022)
15. E. Arslan, F. Kilinc, S. Arzykulov, A.T. Dogukan, A. Celik, E. Basar, A.M. Eltawil, Reconfigurable intelligent surface enabled over-the-air uplink NOMA. IEEE Trans. Green Commun. Netw. **7**, 814–826 (2022)
16. R.A. Tasci, F. Kilinc, A. Celik, A. Abdallah, A.M. Eltawil, E. Basar, RIS-assisted grant-free NOMA (2022). arXiv preprint arXiv:2207.11531

17. M. Aldababsa, A. Khaleel, E. Basar, STAR-RIS-NOMA networks: an error performance perspective. IEEE Commun. Lett. **26**, 1784–1788 (2022)
18. A. Agarwal, R. Chaurasiya, S. Rai, A.K. Jagannatham, Outage probability analysis for NOMA downlink and uplink communication systems with generalized fading channels. IEEE Access **8**, 220461–220481 (2020)
19. C. Pan, H. Ren, K. Wang, W. Xu, M. Elkashlan, A. Nallanathan, L. Hanzo, Multicell MIMO communications relying on intelligent reflecting surfaces. IEEE Trans. Wirel. Commun. **19**(8), 5218–5233 (2020)
20. Y. Ai, A. Felipe, L. Kong, M. Cheffena, S. Chatzinotas, B. Ottersten, Secure vehicular communications through reconfigurable intelligent surfaces. IEEE Trans. Veh. Technol. **70**(7), 7272–7276 (2021)
21. Y. Chen, Y. Wang, J. Zhang, M. Di Renzo, QoS-driven spectrum sharing for reconfigurable intelligent surfaces (RISs) aided vehicular networks. IEEE Trans. Wirel. Commun. **20**(9), 5969–5985 (2021)
22. L. Kong, J. He, Y. Ai, S. Chatzinotas, B. Ottersten, Channel modeling and analysis of reconfigurable intelligent surfaces assisted vehicular networks, in *2021 IEEE International Conference on Communications Workshops (ICC Workshops)* (IEEE, 2021), pp. 1–6
23. M. Ojaroudi, A. Vegni, V. Loscrì, Design and analysis of a reconfigurable intelligent meta-surface for vehicular networks. ITU J. Future Evol. Technol. (2020)
24. H. Guo, Y.-C. Liang, J. Chen, E.G. Larsson, Weighted sum-rate maximization for reconfigurable intelligent surface aided wireless networks. IEEE Trans. Wirel. Commun. **19**(5), 3064–3076 (2020)
25. Z. Lin, H. Niu, K. An, Y. Wang, G. Zheng, S. Chatzinotas, Y. Hu, Refracting RIS-aided hybrid satellite-terrestrial relay networks: joint beamforming design and optimization. IEEE Trans. Aerosp. Electron. Syst. **58**(4), 3717–3724 (2022)
26. H. Niu, H. Lin, K. An, X. Liang, Y. Hu, D. Li, G. Zheng, Active RIS-assisted secure transmission for cognitive satellite terrestrial networks. IEEE Trans. Veh. Technol. **72**, 2609–2614 (2022)
27. Y. Sun, K. An, Y. Zhu, G. Zheng, K.-K. Wong, S. Chatzinotas, H. Yin, P. Liu, RIS-assisted robust hybrid beamforming against simultaneous jamming and eavesdropping attacks. IEEE Trans. Wirel. Commun. **21**(11), 9212–9231 (2022)
28. M.-S. Van Nguyen, D.-T. Do, V.-D. Phan, W. Ullah Khan, A.L. Imoize, M.M. Fouda, Ergodic performance analysis of double intelligent reflecting surfaces-aided NOMA-UAV systems with hardware impairment. Drones **6**(12), 408 (2022)
29. D.-T. Do, D.-T.T. Nguyen, Fixed power allocation for outage performance analysis on AF-assisted cooperative NOMA. J. Commun. **14**(7), 560–565 (2019)
30. T.-L. Nguyen, D.-T. Do, C.X. Mavromoustakis, G. Mastorakis, Opportunistic user selection schemes for energy harvesting-aware cooperative NOMA. Phys. Commun. **44**, 101258 (2021)
31. H. Li, Y. Chen, M. Zhu, J. Sun, D. T. Do, V. G. Menon, P. G. Shynu. Secrecy outage probability of relay selection based cooperative NOMA for IoT networks. IEEE Access, **9**, 1655–1665 (2020)
32. Z. Lin, M. Lin, J.-B. Wang, T. De Cola, J. Wang, Joint beamforming and power allocation for satellite-terrestrial integrated networks with non-orthogonal multiple access. IEEE J. Sel. Top. Signal Process. **13**(3), 657–670 (2019)
33. R. Liu, K. Guo, K. An, S. Zhu, H. Shuai, Noma-based integrated satellite-terrestrial relay networks under spectrum sharing environment. IEEE Wirel. Commun. Lett. **10**(6), 1266–1270 (2021)
34. R. Liu, K. Guo, K. An, F. Zhou, Y. Wu, Y. Huang, G. Zheng, Resource allocation for NOMA-enabled cognitive satellite-UAV-terrestrial networks with imperfect CSI. IEEE Trans. Cogn. Commun. Netw. **9**, 963–976 (2023)
35. J. Pachat, A.A. Mahesh, B.S. Rajan, et al. Index coded-NOMA in vehicular ad hoc networks (2021). arXiv preprint arXiv:2110.11098
36. F. Benabdallah, A. Hamza, M. Becherif, On the use of non-orthogonal multiple access for V2V message dissemination. IET Intell. Transp. Syst. **13**(7), 1125–1129 (2019)
37. K. Guo, R. Liu, M. Alazab, R.H. Jhaveri, X. Li, M. Zhu, STAR-RIS-empowered cognitive non-terrestrial vehicle network with NOMA. IEEE Trans. Intell. Veh. **8**, 3735–3749 (2023)
38. V.B. Kumaravelu, A.L. Imoize, F.R.C. Soria, P.G.S. Velmurugan, S.J. Thiruvengadam, A. Murugadass, V.V. Gudla, Outage probability analysis and transmit power optimization for blind-reconfigurable intelligent surface-assisted non-orthogonal multiple access uplink. Sustainability **14**(20), 13188 (2022)
39. H.K. Jadhav, V.B. Kumaravelu, Blind RIS aided ordered NOMA: design, probability of outage analysis and transmit power optimization. Symmetry **14**(11), 2266 (2022)
40. E. Basar, M. Di Renzo, J. De Rosny, M. Debbah, M.-S. Alouini, R. Zhang, Wireless communications through reconfigurable intelligent surfaces. IEEE Access **7**, 116753–116773 (2019)
41. A. Hemanth, K. Umamaheswari, A.C. Pogaku, D.-T. Do, B.M. Lee, Outage performance analysis of reconfigurable intelligent surfaces-aided NOMA under presence of hardware impairment. IEEE Access **8**, 212156–212165 (2020). https://doi.org/10.1109/ACCESS.2020.3039966
42. E. Basar, Reconfigurable intelligent surface-based index modulation: a new beyond MIMO paradigm for 6G. IEEE Trans. Commun. **68**(5), 3187–3196 (2020)

Publisher's Note